





Cite this: *Mater. Adv.*, 2021,
2, 6369

Antibacterial peptidomimetic and characterization of its efficacy as an antibacterial and biocompatible coating for bioceramic-based bone substitutes†

Sudip Chakraborty,^{‡a} Rajesh Kuppasamy,^{‡*ab} Iman Roohani,^{acd} William R. Walsh,^e Mark D. P. Willcox,^b Naresh Kumar ^a and Renxun Chen ^{*a}

Infection of orthopedic devices by pathogenic bacteria, coupled with the development of bacterial resistance against major antibiotics, have caused severe physical and emotional trauma to patients and posed economic challenges to healthcare institutes and governments worldwide. Antimicrobial peptidomimetics have emerged as promising new candidates to fight the rise of bacterial resistance. Conjugation of these peptidomimetics to bone implant materials has become a viable strategy to combat orthopedic device related infections. In this paper, we report on the synthesis of an anthranilamide-based antibacterial peptidomimetic. The compound, which could possibly be acting through the depolarization of bacterial cell membrane, demonstrated a higher toxicity towards *S. aureus* compared to *E. coli*. We further demonstrated the ability of this compound to disrupt pre-formed biofilms. Coating of the compound on hydroxyapatite discs was achieved via physical interactions between the charged hydroxyapatite surface and the peptidomimetic. This was confirmed via X-ray photoelectron spectroscopy. The compound imparted antibacterial property to the discs as determined via antibacterial assays and imaging, while rendering the discs mildly cytotoxic towards human fetal osteoblast cells.

Received 27th July 2021,
Accepted 29th August 2021

DOI: 10.1039/d1ma00648g

rsc.li/materials-advances

Introduction

Infection of orthopedic implants is a major challenge facing healthcare systems around the world.^{1–3} Infections lead to the failure of implants which necessitates implant revision surgery and, in severe cases, may result in amputation and even mortality.^{4–6} Management of orthopedic implant related infections (ODRIs) also poses a significant financial burden to health care systems and governments.⁷ The rate of infection ranges from 0.7%

to 4.2% in patients that have undergone elective orthopedic surgery, while for patients with trauma that require complex surgeries, the rate can be as high as 30%.^{8–12} Nearly two thirds of all ODRIs are caused by *Staphylococcus* species, of which, *Staphylococcus aureus* and *Staphylococcus epidermis* are the most significant. Between 20% to 30% of ODRIs are caused by *Staphylococcus aureus*.^{13–17} *S. aureus* can make up a significant proportion of the resident microbiota of the skin, and from there can cause hospital- or community-acquired infections.^{18–20}

Treatments of ODRIs have depended heavily on the use of antibiotics. However, one of the major complications with the treatment of ODRIs with traditional antibiotics is the development of bacterial resistance.²¹ The emergence of methicillin resistant *Staphylococcus aureus* has posed serious challenges to established therapeutic protocols for ODRIs.²² A decline in the development of new antibiotics has happened in parallel with the acquisition of resistance to established antibiotics.^{23,24} Just two new antibiotics were developed during 2008–2012.^{25,26} This decline can be attributed to a decrease in antibiotic research, reduced investment in the development of new antibiotics, and unfavorable government regulations.^{27–29}

These developments have necessitated research into alternative strategies to combat bacterial infection. One class of

^a School of Chemistry, UNSW Sydney, 2052, Kensington, NSW, Australia.

E-mail: r.kuppasamy@unsw.edu.au, r.chen@unsw.edu.au; Tel: +61 401426387, +61 406233203

^b School of Optometry and Vision Science, UNSW Sydney, 2052, Kensington, NSW, Australia

^c Charles Perkins Centre, University of Sydney, Sydney, NSW 2006, Australia

^d School of Life and Environmental Sciences, University of Sydney, Sydney, NSW 2006, Australia

^e Prince of Wales Clinical School, UNSW Medicine, UNSW Sydney, Kensington, NSW, Australia

† Electronic supplementary information (ESI) available: Synthesis route and details of each step is provided along with supporting ¹H and ¹³C NMR data. See DOI: 10.1039/d1ma00648g

‡ Equal first authors—Sudip Chakraborty and Rajesh Kuppasamy both contributed equally to the manuscript.

molecules have gained prominence. These are referred to as antimicrobial peptides (AMPs), and are a diverse group of small proteins, some of which play a key role in the innate immune system of various species.³⁰ One of the primary modes of action of AMPs is through the disruption of bacterial cell membranes. AMPs also exert their influence through the modulation of immune responses and the regulation of inflammation.³¹ The primary advantages of AMPs over traditional antibiotics are their broad-spectrum activity and lesser susceptibility towards the development of bacterial resistance.³² There has been a significant amount of research on AMP coated bone implants.^{33–36} Despite a lot of promise, there are certain drawbacks of natural AMPs that hinder their clinical translation. These can include toxicity towards mammalian cells, protease susceptibility,³⁷ sensitivity to changes in pH and salt concentrations,^{38,39} and high costs of production.⁴⁰ These shortcomings have inspired research on mimics of AMPs. Our group has designed short molecule peptidomimetics which have significant antibacterial activity.^{41,42} However, little research has been conducted to demonstrate the application of such peptidomimetics in controlling ODRIs.

Hydroxyapatite (HA) has been used extensively for the fabrication of biomaterials particularly bone substitutes.⁴³ A comparative study of HA based materials with autografts demonstrated increased implant incorporation of the HA graft in a canine model for cervical interbody fusion.⁴⁴ In another study, hydroxyapatite disc fusion exhibited slightly superior performance over autologous iliac crest interbody fusion in anterior cervical disc surgery.⁴⁵ HA has been used as a stand-alone material or in combination with other materials and nanoparticles for the fabrication of bone tissue engineering scaffolds.⁴³ On other occasions, HA has been used as coatings and other formulations to improve the performance of metal and polymer-based implants.^{46–48} Due to its versatility and widespread usage as a material for fabricating bone implants and biomaterials, HA serves as a suitable model material for testing the efficacy of novel antimicrobial peptidomimetics.

In this work, we report the synthesis of a small molecule peptidomimetic and its antibacterial efficacy. We then determine its effectiveness as an antibacterial coating material on hydroxyapatite surface.

Materials and methods

1. Synthesis and characterization of the antimicrobial peptidomimetic

1.1. Synthesis of antimicrobial peptidomimetic compound. Refer ESI† for experimental details.

1.2. Minimum inhibitory concentration (MIC). The antimicrobial activity of the compound was evaluated *via* a broth microdilution assay using the procedure described by Clinical and Laboratory Standards Institute (CLSI). Briefly, *S. aureus* (S.A 38) and *E. coli* (E.C K12) were grown to mid-log phase in Muller Hinton broth (MHB) from Sigma Aldrich, Australia, on a shaker maintaining 120 rpm and inside an incubator, at 37 °C,

for 12–16 h. Following incubation, bacteria were washed three times in PBS, pH 7.4, at 3500 g, for 10 min. After washing, bacteria were diluted with fresh MHB. The turbidity of the bacterial suspension was adjusted such that a value of 0.1 was obtained at the wavelength of 600 nm, which corresponds to a bacterium count of 1×10^8 Colony Forming Units (CFU) mL⁻¹, and then the suspension was further diluted to achieve 5×10^5 CFU mL⁻¹ as the final concentration of bacteria. The compound was diluted (250–3.9 μM) through two-fold dilution. Each dilution of the compound was further added to the wells in a microtiter plate which were also incubated with 100 μL of inoculum containing 5×10^5 CFU mL⁻¹ bacteria. Wells without any compound and containing only bacteria were used as negative controls (*i.e.*, no inhibition of growth). Wells with media only were used as blanks. The microtiter plate was wrapped with paraffin to prevent evaporation and incubated with shaking at 120 rpm and 37 °C for 18–24 h. After incubation, spectrophotometric reading was taken at 600 nm. The concentration of the compound in the well devoid of any visible bacterial growth and an absorbance value of zero was determined to be its MIC.

1.3. Cytoplasmic membrane permeability assay. The method for this assay was adopted from Wu *et al.*⁴⁹ with slight modifications. Bacterial cytoplasmic membrane permeability was determined using membrane potential sensitive dye diSC3-5 (3,3'-dipropylthiadicarbocyanine iodide) whose penetration inside bacterial cells depends on the potential gradient across their cytoplasmic membranes. Bacteria (S.A 38 and E.C K12) were grown in MHB to mid-log phase *via* shaking at 37 °C inside an incubator for 18–24 h. Following incubation, bacteria were washed with a 5 mM HEPES (pH 7.2) solution containing 20 mM glucose and then resuspended in the same buffer to a final optical density of about 0.5–0.6 at 600 nm, which approximately corresponds to a bacterium count of 1×10^7 CFU mL⁻¹. The dye diSC3-5 was added at a concentration of 4 μM to the bacterial suspensions. The suspensions were incubated in the dark and at room temperature for 1 h to ensure maximum dye uptake by the bacterial cells. Then, 100 mM KCl was added to balance the K⁺ concentration across the bacterial cell membrane to prevent further uptake or outflow of the dye. For the Gram-negative bacteria, 0.5 mM EDTA was used to destabilize the lipopolysaccharides–Mg²⁺–Ca²⁺ complex to help in the penetration of the dye without affecting bacterial growth. 100 μL of bacterial suspension was added to a 96-well microtiter plate with equal volume of antimicrobial compound. Three different concentrations of the antimicrobial compound were tested in this experiment. The concentrations (1× MIC, 2× MIC, 4× MIC) were selected based on the MIC values determined in the previous experiment, where 1×, 2×, and 4× MIC denote one-fold, two-fold, and four-fold MIC, respectively. DMSO (20%) was used in the growth media as positive control while bacteria grown in the absence of any compound was used as untreated control. Fluorescence was measured with a luminescence spectrophotometer at 3 min intervals at an excitation wavelength of 622 nm and an emission wavelength of 670 nm.

1.4. Biofilm disruption assay. Bacterial cultures (S.A 38 and E.C K12) were grown in MHB overnight at 37 °C with shaking at



120 rpm. Cultures were diluted (1:20) in MHB medium and 200 μL aliquots were dispensed to flat bottom 96-well plate wells (Sarstedt Australia). Biofilm was allowed to grow in the 96-well plate for 24 h, followed by the addition of the compound and further incubation for 24 h. Four different concentrations of the compound; 1 \times , 2 \times , 4 \times , 8 \times MIC, corresponding to one-fold, two-fold, four-fold, and eight-fold MIC were chosen for this study. Untreated biofilm was used as control. Plates were sealed with self-adhesive microplate sealers (TopSeal-A, PerkinElmer) to allow diffusion of air and to prevent condensation. Biofilms adhered on polystyrene substratum were quantified by crystal violet staining as described previously.⁵⁰ This experiment was performed in triplicate.

2. Synthesis of HA nanoparticles and discs

2.1. Synthesis of HA nanoparticles. Hydroxyapatite nanoparticles were synthesized according to a protocol developed in our group. Briefly, 236.15 grams of calcium nitrate tetrahydrate and 79.236 grams of ammonium phosphate dibasic were weighed and added to two separate beakers containing MilliQ water (1500 mL for calcium nitrate tetrahydrate and 500 mL for ammonium phosphate dibasic). The solution containing calcium nitrate tetrahydrate was heated on a hot plate. Ammonium phosphate dibasic was allowed to completely dissolve in solution and then it was added to the calcium nitrate tetrahydrate solution after the latter reached a temperature of 60 °C. The solutions were mixed slowly in order to maintain a pH of above 7.5 throughout the mixing process. After complete mixing, the final 2000 mL solution was passed through a filter paper. The solvent was discarded, and the paste consisting of HA nanoparticles was retained and allowed to dry overnight. The HA nanoparticles were then sintered at four different temperatures for one hour. The selected temperatures were 800 °C, 1000 °C, 1050 °C, and 1100 °C. The sintered nanoparticles were then observed under SEM.

2.2. Synthesis of HA discs. HA nanoparticles synthesized in the previous step were used for the fabrication of discs. Briefly, the sintered nanoparticles were first ground and disaggregated using a mortar and a pestle. The ground nanoparticle powder was then passed through a 0.2 μm sieve to retain particles larger than that for further grounding. The particles smaller than 0.2 μm were mixed with water at 40 wt% (40 grams of nanoparticles in 60 grams of water). The water-nanoparticle mixture was then homogenized in a ball mill for 60 minutes. The homogenized mixture was then cast into cylindrical molds and allowed to dry overnight in a desiccator. The dried cylindrical HA discs were then sintered at 1100 °C for 6 hours. The surface morphology of the sintered HA discs was analyzed using Scanning Electron Microscopy (SEM).

3. Synthesis and physical characterization of peptidomimetic coated hydroxyapatite discs

3.1. Synthesis of peptidomimetic coated HA discs. Peptidomimetic was coated onto the HA discs *via* physical adsorption. Briefly, sintered HA discs were incubated in an aqueous solution containing the peptidomimetic for 24 hours under

mild shaking condition at room temperature. For this purpose, three different solutions of the peptidomimetic were prepared in water, each having a concentration of 100 $\mu\text{g mL}^{-1}$, 500 $\mu\text{g mL}^{-1}$, and 1000 $\mu\text{g mL}^{-1}$ peptidomimetic, respectively. After incubation, the solutions were removed, and the discs were washed thrice with distilled water in order to remove loosely bound and unbound peptidomimetics. The discs were then allowed to dry at room temperature for roughly 18–24 hours. These coated discs were used for subsequent experiments.

3.2. UV-Vis spectroscopy. The amount of peptidomimetic attached to the HA discs was measured indirectly through UV-Vis spectroscopy. This was done immediately after attachment of the peptidomimetic to the discs. As mentioned in the previous step, HA discs were incubated in the peptidomimetic solutions for 18–24 hours for effective adsorption. After the incubation, the solution was removed and its absorbance was measured at 260 nm. Before this, a standard curve of the peptidomimetics concentration vs absorbance was generated. The value of absorbance obtained in the solutions was then compared to this standard curve to determine the concentration of peptidomimetic left in it. The amount of peptidomimetic attached to the discs was calculated as $\{C_i - C_f\} \times V$, where C_i is the initial concentration of the peptidomimetic in the solution, C_f is the concentration after 24 hours of incubation of HA disc in the solution, and V is the volume of the solution.

3.3. X-Ray photoelectron spectroscopy (XPS). The surface of uncoated and peptidomimetic coated HA discs were analyzed *via* XPS to qualitatively determine the adsorption of the peptidomimetic. A Thermo ESCALAB250Xi X-ray photoelectron spectrometer was used at a background vacuum higher than 2×10^{-9} mbar. A mono-chromated Al K α (energy 1486.68 eV) was used as the X-ray source and the power was maintained at 120 W. A photoelectron take-off angle of 90° and a spot size of 500 μm was chosen for the analysis.

3.4. Fourier transform infrared spectroscopy (FTIR). The HA discs (uncoated and coated) were further analyzed *via* FT-IR spectroscopy. A Spectrum 100/Spotlight 400 FT-IR spectrometer was used for the analysis. The scanning range was set from 650 to 4000 cm^{-1} .

3.5. RAMAN spectroscopy. The discs were also analyzed *via* RAMAN spectroscopy. Uncoated HA discs and HA discs coated with the three different concentrations of the peptidomimetic were used in the analysis. A standard diode laser setting of 532 nm (green) was used along with a grating of 1800 l mm^{-1} . The scanning range was set from 44 to 1826 cm^{-1} .

4. In vitro antimicrobial evaluation of peptidomimetic coated discs

4.1. Direct contact antibacterial assay. Antibacterial activity of the discs was evaluated *via* directly growing bacteria on their surfaces.⁵¹ Briefly, a stock solution of *S. aureus* 38 was prepared by incubating MHB with the bacteria and growing it overnight at 37 °C. *S. aureus* 38 for this step was isolated by picking a single colony from a freshly prepared streak plate.



After incubation, the *S. aureus* 38 containing MHB was centrifuged at 3500 rpm for 10 minutes in an Eppendorf 5430 multifaceted centrifuge. Subsequently, the supernatant was discarded, and the pellet was dissolved in fresh MHB. The amount of MHB added to the pellet was adjusted such that the absorbance value of the solution, when observed in a microplate reader at 600 nm, read 0.1. This is corresponding to a bacterial concentration of 10^8 CFU mL⁻¹. After adjustment of the absorbance, the media was further diluted 1000-fold to reach a final bacterial concentration of 10^5 CFU mL⁻¹. Peptidomimetics coated discs, in triplicates, were placed in 96 well plates. Uncoated discs were used as controls. These discs were submerged in the diluted media and incubated overnight at 37 °C. After the incubation, media from each well were collected into separate Eppendorf tubes and diluted serially with PBS from 1 to 10-fold. All the dilutions corresponding to media collected from an individual well were then plated in an agar plate. These plates were incubated overnight at 37 °C. The number of colonies at each dilution were counted the next day, and the CFUs mL⁻¹ of the corresponding undiluted media was calculated as CFUs mL⁻¹(undiluted media) = CFUs in *n*th dilution $\times 10^n$.

4.2. Bacterial adhesion assay. The number of bacteria attached to the surface of the discs was quantified using a modification of the aforementioned protocol.⁵² Coated discs were submerged in 10^5 CFUs mL⁻¹ of *S. aureus* 38 containing media and incubated overnight at 37 °C. Subsequently, the media was removed, and the discs were washed thrice with PBS with mild shaking for 5 minutes. The washing steps ensure the removal of loosely attached bacteria. After the third wash, the discs were submerged again in media and vortexed vigorously for 5 more minutes. This was done to dissociate the strongly attached bacteria from the discs. The media was then collected in an Eppendorf tube and serially diluted from 1 up to 10-fold. Each dilution was then plated on separate agar plates and incubated overnight at 37 °C. The number of colonies corresponding to each dilution was counted on the following day and the CFUs mL⁻¹ in the corresponding undiluted media was back calculated according to the following formula CFUs mL⁻¹(undiluted media) = CFUs in *n*th dilution $\times 10^n$.

5. In vitro cytotoxicity

5.1. Cell culture. The *in vitro* cytotoxicity studies were performed with human fetal osteoblastic cell line hFOB 1.19. For this purpose, cells previously frozen in our lab at passage 4 were thawed and subsequently revived in DMEM/F-12 media supplemented with 10% Fetal Bovine Serum (FBS), and penicillin (5000 unit per mL), and streptomycin (5000 µg mL⁻¹). The cells were grown by incubation in a humidified CO₂ chamber that was maintained at 5% CO₂ and 37 °C. The cells were grown for one more passage before they were used for the subsequent experiments.

5.2. Alamar blue assay. The cytotoxicity of the scaffolds was determined by measuring the metabolic rate of hFOB 1.19 cells grown on the scaffolds for 24 and 72 hours in an alamar blue assay. Briefly, uncoated and peptidomimetic coated scaffolds

were incubated in DMEM/F-12 media supplemented with 10% FBS for 24 hours. Before cell seeding, the scaffolds were replenished with fresh media. The cells for this purpose were obtained *via* trypsinization of a monolayer cultured in tissue culture flasks as mentioned above. The trypsinized cell suspension was seeded onto the scaffolds at a density of 10^4 cells per scaffold. After 24 and 72 hours of culture on the scaffolds, alamar blue reagent was added such that the final media contained 10% alamar blue reagent (v/v). After addition, the cells were further incubated for 2 hours at 37 °C in a humidified CO₂ chamber. After the incubation, the media was transferred to a 96 well microtiter plate and the absorbance of the media was measured at 570 nm with 600 nm as the reference. The metabolic activity of the cells was taken as a measure of their viability, and it was calculated from the absorbance values as follows:

$$\text{Percentage cell viability} = \frac{(M_2 \times A_1) - (M_1 \times A_2)}{(M_2 \times P_1) - (O_1 \times P_2)} \times 100,$$

where: M_1 = molar extinction coefficient (E) of oxidized alamar blue (blue) at 570 nm, M_2 = molar extinction coefficient (E) of oxidized alamar, blue (blue) at 600 nm, A_1 = absorbance of test wells at 570 nm, A_2 = absorbance of test wells at 600 nm, P_1 = absorbance of positive growth control well (cells in tissue culture plate) at 570 nm, P_2 = absorbance of positive growth control well at 600 nm.

5.3. SEM imaging. The morphology of the cells growing on the surface of the HA discs was determined *via* imaging the surface of the discs under a SEM. For this purpose, cells were grown on the surface of the discs for 24 hours as mentioned previously. After 24 hours of growth, the cell culture media was removed, and the surface of the discs was wiped with PBS. Then, the discs were incubated in a 2.5% glutaraldehyde solution for 2 hours in a humidified CO₂ chamber maintained at 37 °C. After the incubation, the glutaraldehyde solution was discarded and the discs were serially washed with solutions of increasing ethanol concentrations (starting from 50%, then 60%, going all the way to 100%). Each washing step involved incubation of the discs in the respective ethanol solution for 10 minutes at room temperature. After the final wash, the discs were dried in a critical point dryer. The dried discs were subsequently sputter coated with platinum and taken for imaging. NanoSEM 230 was operated at an accelerating voltage of 3 kV and a spot size of 3 for the imaging.

The morphology of the bacteria attached to the discs was observed under SEM. The same protocol as above was followed for fixing the cells. NanoSEM 230, a field-emission scanning electron microscope (FE-SEM) was used for the imaging. The spot size was fixed at 3 and an accelerating voltage of 10 kV was used for the imaging.

Statistics. The bar graphs are plotted as mean \pm standard deviation. Unless specified otherwise, all the experiments were performed in triplicates and repeated at least three independent times. The data was analyzed *via* one way Analysis of Variance (one way ANOVA). A *p*-value of less than 0.05 was considered to be statistically significant.



Results

1. Synthesis and characterization of novel antimicrobial peptidomimetic for surface coating

We have previously reported amphiphilic anthranilamide compounds as antimicrobial peptidomimetics.⁴¹ In this study, we have designed a cationic synthetic peptide for noncovalent, electrostatic binding with HA, aiming to construct an antimicrobial coating. Amongst the different biaryl compounds that were synthesized (data not presented), one compound (**6** in Scheme 1) was found to be active against *S. aureus* (MIC = 3.9 μ M) and *E. coli* (MIC = 31.2 μ M). The compound was further investigated to understand its mode of action. As most AMP mimics kill bacteria by disrupting their cytoplasmic membranes, membrane permeability assays are illuminating for analyzing their mode of action.⁵³ The membrane potential-sensitive dye cyanine disC3-5 (3,3'-dipropylthiadicarbocyanine iodide) assay was used to analyze the ability of our compound to depolarize the cytoplasmic membrane of *S. aureus* and *E. coli*. Perturbation of the bacterial cell membrane by a membrane disruptive compound leads to the loss of the membrane potential gradient, thereby causing the dye to be released into the medium. The release of the dye subsequently increases the fluorescence intensity of the medium, which can be used as a measure of membrane activity of the compound. The addition of biaryl compound **6** at 1 \times MIC (3.9 μ M) against *S. aureus* rapidly increased the fluorescence intensity indicating the perturbation of the cell membrane (Fig. 1(a)). Similar results were obtained when the cytoplasmic permeability assay was performed on *E. coli* as well (Fig. 1(b)).

Biofilms have been shown to be 10–1000 times more resistant to conventional antibiotics.⁵⁴ We tested the ability of our peptidomimetic compound for its ability to disrupt established *S. aureus* and *E. coli* biofilms using the crystal violet staining assay. The ability of compound **6** to disrupt the biofilms was measured at increasing concentrations that were multiples of its MIC; 1 \times , 2 \times , 4 \times , and 8 \times , where \times is the MIC of compound **6** (Fig. 2). Compound **6** disrupted around 93% of biofilm at 4 \times MIC (15.6 μ M) concentration. However, the compound did not show biofilm disruption of *E. coli* even at a concentration of >125 μ M, corresponding to 32 \times MIC.

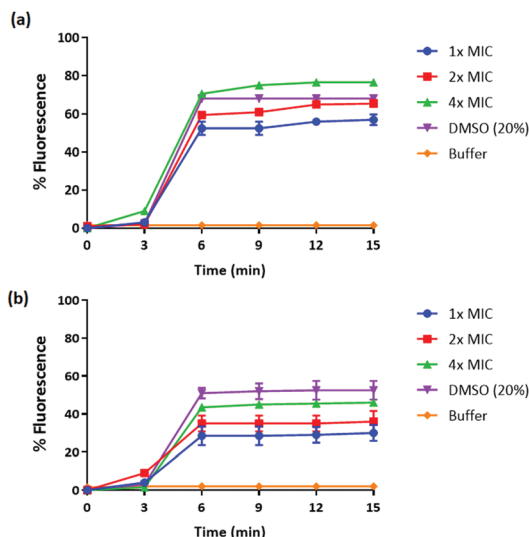


Fig. 1 Cytoplasmic membrane depolarization of (a) *S. aureus* 38 and (b) *E. coli* K12 by **6**, as assessed by release of the membrane potential-sensitive dye DiSC3-(5) measured spectroscopically at 622 nm and 670 nm, as the excitation and emission wavelength respectively. 1 \times , 2 \times , and 4 \times MIC denote one-fold, two-fold, and four-fold MIC, respectively. Data presented as means (\pm SD) of three independent repeats in triplicate cells 20% DMSO was used as a positive control.

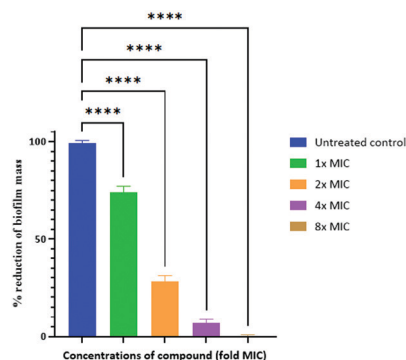
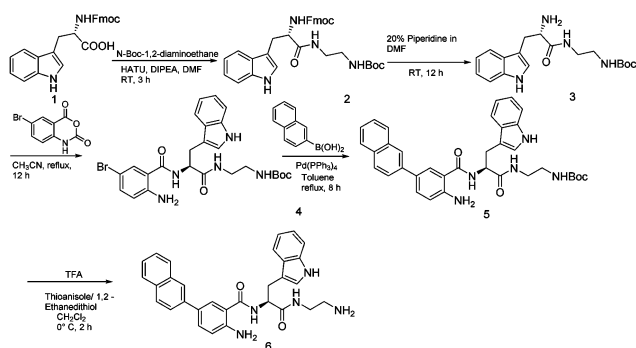


Fig. 2 Disruption of established biofilm of *S. aureus* after 24 h with 1 \times to 8 \times MIC concentrations of compound **6**. 1 \times , 2 \times , 4 \times , and 8 \times MIC denote one-fold, two-fold, four-fold and eight-fold MIC, respectively. The positive control represents the preestablished biofilms without any compounds. **** = p -value < 0.0001.



Scheme 1 Synthesis of antibacterial peptide mimics for surface coating.

The active peptidomimetic compound was further assessed for its activity after attachment on HA discs.

2. Synthesis of HA nanoparticles and discs

2.1. Synthesis of HA nanoparticles. HA nanoparticles were synthesized *via* a protocol developed in our group. After sintering at four different temperatures, the morphology of the nanoparticles was observed under SEM (Fig. 3). The nanoparticles appeared aggregated under the microscope and the nanoparticles sintered at 1000 $^{\circ}$ C displayed a morphology more suitable for fabrication of discs (Fig. 3(c)). These nanoparticles were chosen for the synthesis of HA discs and all the subsequent experiments.

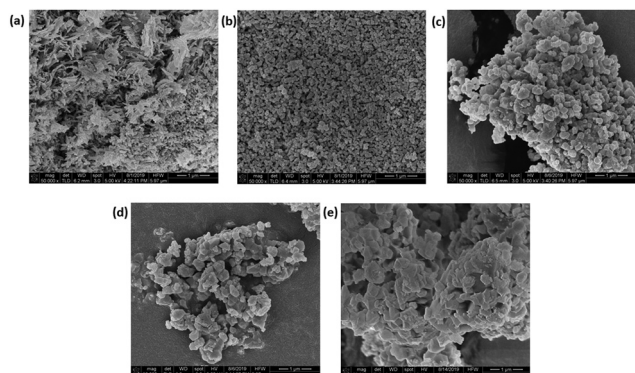


Fig. 3 Scanning electron micrographs of (a) un-sintered and (b)–(e), HA nanoparticles sintered at 800, 1000, 1050, and 1100 °C, respectively.

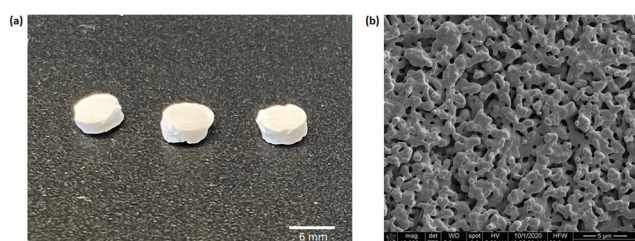


Fig. 4 (a) Sintered HA discs, (b) scanning electron micrograph of HA disc surface.

2.2. Synthesis of HA discs. HA discs were prepared by drying a 40 wt% solution of HA inside cylindrical PMMA molds and subsequent sintering at 1000 °C. The discs appeared mechanically rigid to naked eyes (Fig. 4(a)). The surface of the discs, as elucidated through SEM, appeared porous (Fig. 4(b)). This porosity is most likely to be a characteristic feature of the entire volume of the disc.

3. Synthesis and characterization of peptidomimetic coated HA discs

3.1. Synthesis of peptidomimetic coated HA discs. Peptidomimetic coated discs were synthesized *via* physical adsorption of the peptidomimetic onto the HA discs. Uncoated and coated discs were imaged under an SEM (Fig. 5(a)–(d)). Incubation of the discs in peptidomimetic solution did not alter their surface morphology as can be seen from the SEM images.

3.2. UV-Vis spectroscopy. The degree of peptidomimetic attachment on the HA discs was quantified indirectly through UV-Vis spectroscopy. A dose dependent increase was observed in the amount of peptidomimetic attached to the discs (Fig. 5(e)). The amount of peptidomimetic attached to the discs was approximately 5, 28, and 55 µg, corresponding to loading concentrations of 100, 500, and 1000 µg mL^{−1} respectively.

3.3. X-Ray photoelectron spectroscopy (XPS). Surface elemental composition of uncoated and coated HA discs was determined through XPS. An increase in the total carbon coverage on the surface was observed with an increase in the peptidomimetic loading (Fig. 6(a)). Uncoated HA disc had a

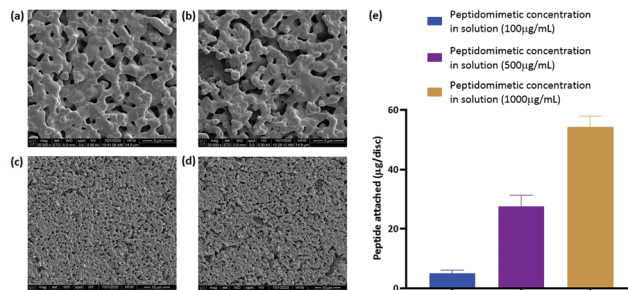


Fig. 5 (a) and (c) Scanning electron micrographs of HA discs incubated in water for 24 h and (b) and (d) incubated in 1000 µg mL^{−1} peptidomimetic solution for 24 h. (e) Quantification of peptidomimetic attachment on HA discs corresponding to three different concentrations of peptidomimetic loading solution. *n* = 3.

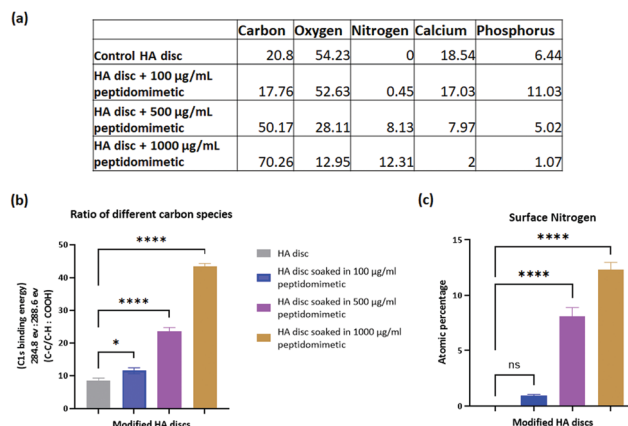


Fig. 6 (a) Surface elemental composition of the uncoated and coated HA discs, (b) ratio of different carbon species on the surface of the discs, (c) surface coverage of nitrogen on the discs. ns = no significance, * = *p*-value < 0.5, **** = *p*-value < 0.0001. *n* = 3.

surface Carbon coverage of 20.8% while HA discs soaked in 100, 500, and 1000 µg mL^{−1} peptidomimetic had surface carbon coverages of 17.76, 50.17, and 70.26% respectively. Upon further inspection of the total carbon content, at least four different types of carbon species were found corresponding to carbon present in different types of bonds. Out of these, two types of carbon species were of interest to us: carbon present in C–C/C–H bonds (corresponding to a binding energy of 284.8 eV, Fig. 6(b)) and carbon present in COOH groups (corresponding to a binding energy of 288.6 eV, Fig. 6(b)). Accumulation of COOH on the surface is due to adsorption of adventitious carbon from the environment while preparation and handling of the discs. C–C/C–H is contributed by the peptidomimetic and its accumulation on the surface is an indication of the adsorption of the peptidomimetic on the surface. We observed an increase in the ratio of C–C/C–H relative to COOH with an increase in peptidomimetic loading on HA discs indicating an increase in the amount of adsorbed peptidomimetic with an increase in initial loading. The total nitrogen coverage on the surface also increased with an increase in the initial peptidomimetic loading (Fig. 6(c)). The



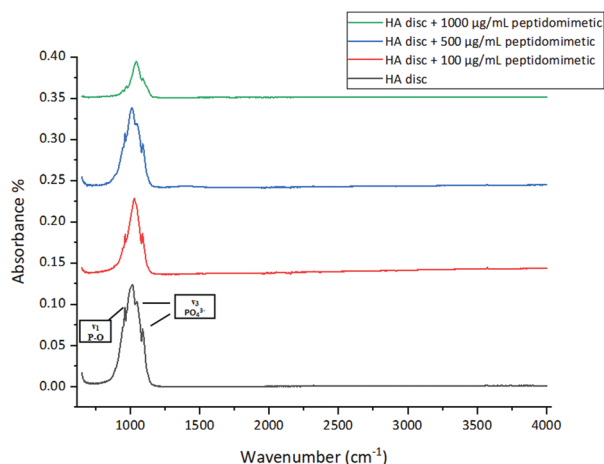


Fig. 7 FT-IR spectra of unmodified and modified HA discs.

surface nitrogen is contributed solely by the peptidomimetic, and therefore, an increase in the surface nitrogen coverage further confirms the adsorption of the peptidomimetic to the surface.

3.4. Fourier transform infrared spectroscopy (FTIR). The FT-IR spectrum of the uncoated and coated HA discs showed the characteristic HA peaks (Fig. 7). In the spectra of the uncoated and the three coated discs, the peaks around 960 cm^{-1} correspond to ν_1 nondegenerate symmetric stretching characteristic of P-O bonds. Furthermore, the peaks associated with ν_3 vibration mode of the PO_4^{3-} are observed around 1036 and 1095 cm^{-1} .

All the four spectra follow the characteristic spectrum of HA; however, the intensity and sharpness of the peaks decreased with an increase in the amount of bound peptidomimetic.

3.5. RAMAN spectroscopy. The surfaces of the discs were further analyzed *via* RAMAN spectroscopy. Similar to the spectra in FT-IR, all the four RAMAN spectra showed the characteristic spectrum of HA (Fig. 8). The peaks at 1076 cm^{-1} , 1046 cm^{-1} , 1030 cm^{-1} , and 961 cm^{-1} correspond to the

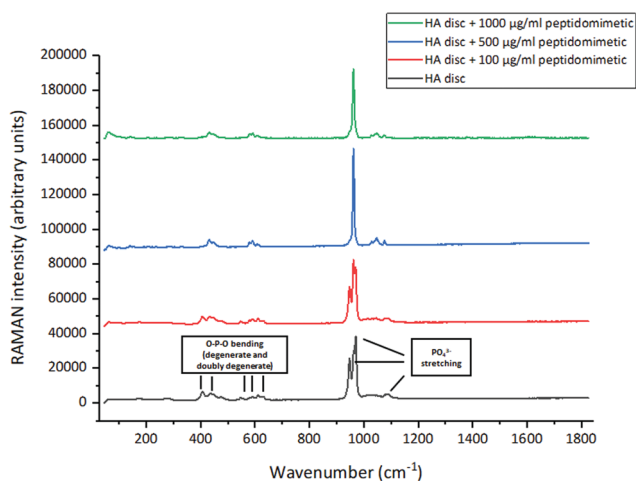


Fig. 8 RAMAN spectra of unmodified and modified HA discs.

asymmetric and symmetric stretching modes of the PO_4 group. The peaks observed around 610 cm^{-1} , 594 cm^{-1} , and 582 cm^{-1} correspond to the triply degenerated bending mode of the O-P-O bond. Furthermore, the peaks at 433 cm^{-1} and 447 cm^{-1} correspond to the doubly degenerated bending mode of the same bond. The intensity and sharpness of some of these peaks and bands decrease with an increase in the amount of adsorbed peptidomimetic on the surface of the discs.

4. Antibacterial adhesion assay

The antibacterial activity of the peptidomimetic coated discs was evaluated in a direct contact antibacterial assay.³⁶ The coated discs demonstrated higher antibacterial activity than the uncoated control discs, exhibiting a 2 log reduction in the number of viable bacteria in the media (Fig. 9(a)). However, a significant dose dependent increase in the antibacterial activity of the coated discs was not observed. A trend towards an increasing activity was noticed but the differences between groups with different amounts of loaded peptide were not statistically significant.

The number of bacteria attached to the discs was quantified by a slight modification of the protocol of the direct contact antibacterial assay. A reduction in the total number of bacteria attached to the discs was observed between the coated and the uncoated discs (Fig. 9(b)). However, like the case with bacteria in media, no significant difference was observed within the three different coated discs.

The morphology of the attached bacteria was observed under SEM. S.A. 38 exhibited a spherical morphology on all the discs and no structural deformities were visible on the bacteria grown on the coated discs (Fig. 10). The number of bacteria within a field of view was higher in the uncoated disc compared to that on the coated discs.

5. In vitro cytotoxicity

5.1. Alamar blue assay. The cytotoxicity of the discs was measured *via* alamar blue assay. A dose dependent increase in cytotoxicity was observed with increasing amounts of the peptidomimetic on the discs (Fig. 11). However, the magnitude of cytotoxicity on all the discs was within the acceptable range. Unmodified HA discs had a toxicity level closest to the tissue culture plate control (approximately 95% cell viability). Amongst the coated discs, the discs loaded with $5\text{ }\mu\text{g}$ of

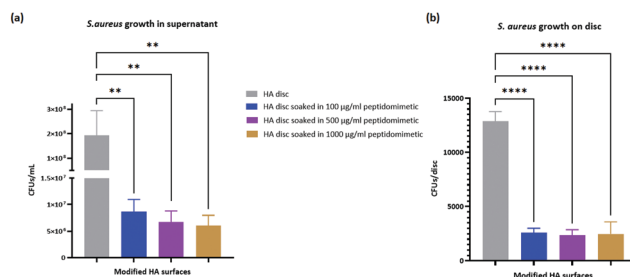


Fig. 9 (a) CFUs in supernatant, (b) CFUs on disc surface. ** = p -value < 0.01 , *** = p -value < 0.0001 . $n = 3$.



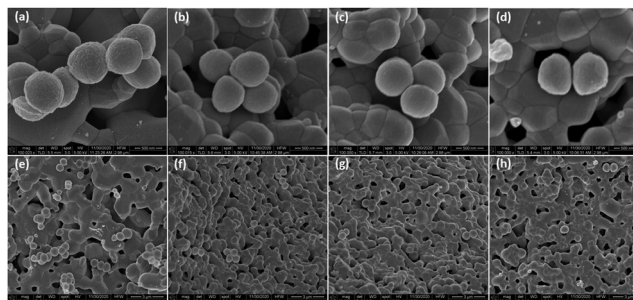


Fig. 10 SEM micrographs of *S. aureus* on the surfaces of (a) HA disc, (b)–(d) HA disc soaked in 100, 500, 1000 $\mu\text{g mL}^{-1}$ peptidomimetic, respectively. (e)–(h) corresponding images of the same samples in the same order at a lower magnification.

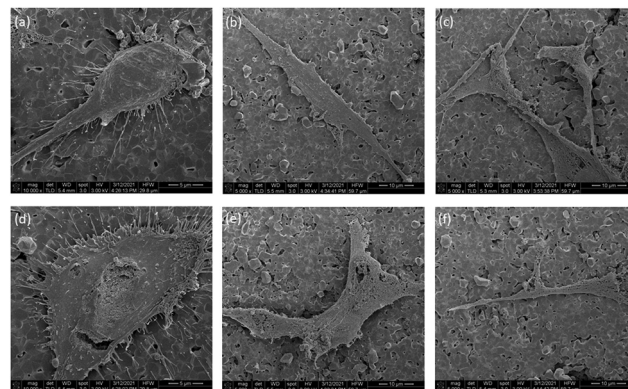


Fig. 12 SEM of hFOB on (a)–(c), HA disc, (d)–(f), HA disc soaked in 100 $\mu\text{g mL}^{-1}$ peptidomimetic.

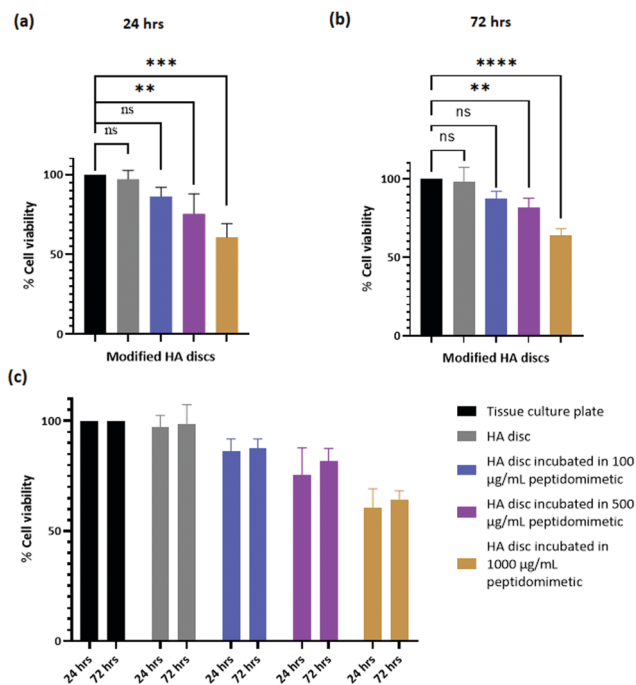


Fig. 11 Cytotoxicity after (a) 24 h, (b) 72 h of cell culture on discs, (c) side by side comparison of cytotoxicity at 24 and 72 hours, respectively. ns = no significance, ** = p -value < 0.01 , *** = p -value < 0.001 , **** = p -value < 0.0001 . $n = 3$.

peptidomimetic demonstrated quite low cytotoxicity (approximately 86% cell viability), while discs loaded with 28 and 55 μg of peptidomimetic showed significant cytotoxicity (approximately 75 and 63% cell viability, respectively). The increase in cytotoxicity with an increased peptidomimetic loading could possibly be due to the membrane disruptive effect of the peptidomimetic, although further studies need to be performed to explore the mechanism of cytotoxicity. Since the antibacterial activity of the discs loaded with three different concentrations of the peptidomimetic is quite comparable and the disc loaded with the lowest amount of peptidomimetic has negligible cytotoxicity, we decided to take a disc with the lowest amount of peptidomimetic for morphological analysis of the cells growing on the discs.

5.2. SEM imaging. The morphology of the cells growing on the discs was observed through SEM. The cells appeared healthy after 24 hours of growth on both uncoated and HA discs coated with 5 μg peptidomimetic (Fig. 12(d)–(f)). They displayed an elongated morphology with projections extending out of the cellular body as is observed for healthy osteoblasts growing under normal osteogenic conditions.

Discussion

The prevalence of bacterial infections on orthopedic implants and biomaterials is a major challenge for governments and healthcare institutes around the world. The presence of *S. aureus* in a significant majority of these infections makes it a major target of therapeutic interventions. However, traditional antibiotics, despite their success, have become ineffectual in treating a lot of infections due to the emergence of antibiotic resistance in bacteria. Novel strategies for treating infections have utilized AMPs and their synthetic analogs. Natural AMPs are not particularly suitable for use in the pharmaceutical industry due to their drawbacks mentioned before. Synthetic mimics of AMPs, also known as antibacterial peptidomimetics, retain crucial structural features of AMPs responsible for their antibacterial activity while overcoming some of their drawbacks.

Our group has previously reported amphiphilic anthranilamide compounds as novel antibacterial peptidomimetics.^{41,42} Inspired by the success of those compounds, our current work describes the synthesis of a novel antibacterial peptidomimetic for potential application as a coating material for orthopedic devices. In this paper, we reported on the synthesis of a new anthranilamide-based peptidomimetic. The compound demonstrated activity against both Gram-positive and Gram-negative bacteria and its MIC against *S. aureus* 38 strain was significantly lower than its MIC against *E. coli* K12 strain. One possible common mechanism of action of AMPs and AMP mimics is the disruption of bacterial cell membrane. Membrane disruption is initiated by the attachment of the AMPs and their mimics to the membrane surface which is



facilitated by the cationic and amphiphilic nature of these molecules. Our compound demonstrated the ability to destabilize artificial membrane in the cytoplasmic membrane permeability assay, which suggests that membrane disruption is an integral part of mechanism of action for the peptidomimetic. This can be attributed to the cationic and amphiphilic nature of our compound which, as mentioned before, are crucial parameters determining the attachment of antibacterial entities to the surface of bacterial membranes. Furthermore, our compound demonstrated the ability to disrupt pre-formed biofilms. These results suggest that the peptidomimetic is a suitable candidate for the prevention and/or treatment of bacterial infections.

One of the strategies for combatting orthopedic device associated infections is the release of antibacterial agents from the devices *in situ*. Biomaterials and devices used in orthopedic therapy have been coated with antibacterial entities, both traditional antibiotics and AMPS/peptidomimetics.^{55–57} Amongst the different coating strategies, direct covalent and non-covalent attachment of antibacterial entities to surfaces have been explored quite extensively.^{36,58} Non-covalent attachment strategies leverage the charged and/or polar properties of some drugs and material surfaces to form favorable weak interactions between the two. This type of attachment is reversible and the characteristics of the material and the antibacterial entity contributing to their interaction can be modified to tune the strength of attachment and dissociation kinetics. Non-covalent attachment of an antibacterial entity on a biomaterial surface also allows for sustained release of the antibacterial over a prolonged period.

To investigate the utility of the peptidomimetic as antibacterial coating, we evaluated the efficacy of non-covalently attached peptidomimetic coating on HA discs. HA is a biocompatible and osteoconductive material used extensively in repair of bone defects. It serves as a good model material for testing the efficacy of novel antibacterial agents as coatings for biomaterials used in orthopedics. For our studies, we prepared cylindrical HA discs using HA nanoparticles. Cylindrical discs are easy to handle and transport for experimental purposes and the results obtained from them can be generalized to other HA based formulations, provided the surface properties of HA remain intact and play a dominant role in the function of the material. HA nanoparticles with approximately spherical morphology were selected for the formulation of the discs.

HA has a negatively charged surface at physiological pH. Studies have reported on the effect of solution pH on the charge of HA surfaces, and although there is some variability in the data owing to the different sources and fabrication techniques of HA used in these studies, the isoelectric point, and the point of zero charge of HA have been found to be below 7 in most cases. Thus, at pH 7, HA has a net negative charge on its surface, which has been found to be favourable for protein adsorption.⁵⁹ This surface property makes physical adsorption of charged antibacterial entities a viable route of infection therapy. We took advantage of the cationic nature of our peptidomimetic to bind it physically through electrostatic

interaction to the surface of HA discs. The binding was confirmed *via* XPS. The adsorption of the peptidomimetic on the surface led to an increase in the nitrogen and a specific type of carbon (C–C/C–H) content on the surface. Some of the surface carbon was attributed to nonspecific adsorption of contaminants from the environment (adventitious carbon), however, the proportion of the adventitious carbon within the total carbon species reduced as more peptidomimetic attached to the surface, and the major fraction of the surface carbon was attributed to the peptidomimetic. Binding of the peptidomimetic to the discs did not interfere with the native functional groups present within HA, as was demonstrated *via* FT-IR and RAMAN spectroscopy. The lack of peaks specific to the peptidomimetic in the FT-IR and RAMAN spectra of the discs could be attributed to the formation of a very thin layer of coating, below the detection limit of the two spectroscopic methods.

We subsequently evaluated the antibacterial activity of the discs. Preliminary evaluation of antibacterial activity was done *via* a Kirby–Bauer disc diffusion assay (data not shown). A visible zone of inhibition in a lawn of *S. aureus* surrounding the peptidomimetic coated discs indicated the presence of antibacterial activity in the discs. To characterize the activity further, we went ahead with direct contact antibacterial assays and quantified the decrease in the number of viable *S. aureus* on the surface of coated discs and their surrounding medium compared to the number of viable *S. aureus* on uncoated HA disc and its surrounding medium. A significant decrease in the number of viable *S. aureus* was observed both on the surface of the coated discs and their surrounding medium compared to their uncoated counterparts, indicating the retention of antibacterial activity of the peptidomimetic on HA surface and also its release into the surrounding medium. The magnitude of decrease in viable bacteria in our study is comparable to those described in previous publications with different AMPs and peptidomimetics.^{36,60} These results look promising and further characterization of the peptidomimetic HA interactions can be performed to optimize their interactions. Simultaneously, structural analogs of the peptidomimetic used in this study can be synthesized and assessed for their efficacy.

In order for satisfactory regeneration of bone, biomaterials and implants used in orthopedic reconstruction should allow the growth of cells (osteoblasts and stem cells) on their surfaces. HA is intrinsically osteoconductive and therefore, provides a favorable environment for osteoblasts to attach and proliferate. Alamar blue assay was performed to assess the cytotoxicity of the coated discs and SEM imaging was performed to visualize the morphology of the cells on the discs. hFOB 1.19 cells were chosen for these studies as it is a widely accepted cell line for modeling the behavior of human osteoblasts. Incorporation of our peptidomimetic rendered the discs cytotoxic in a dose dependent manner. However, the magnitude of the cytotoxicity is within the acceptable range for biomaterials. Furthermore, the discs with the lowest amount of peptidomimetic yielded a cytotoxicity value that wasn't significantly different to the uncoated HA discs. The morphology of the cells was unaffected by the incorporation of the peptidomimetic as



can be inferred from the SEM images. It is plausible that contact with the peptidomimetic coated discs alters the metabolic rate of the cells and this resulted in a reduced viability count. However, the behavior of osteoblasts in contact with these discs needs to be studied further to reach a conclusion on the mechanism of cytotoxicity.

Conclusions

We have successfully designed a novel antibacterial peptidomimetic. The possible mode of action of this compound is *via* the disruption of the bacterial cell wall. Its antibacterial activity against *S. aureus* suggests its possible applicability towards the treatment of orthopedic device related infections. By coating the surface of HA discs with the peptidomimetic and then testing the antibacterial efficacy and cytotoxicity of the coated discs, we have determined the propensity of the peptidomimetic to attach to HA *via* electrostatic interactions and the compound retains its activity after the attachment. This study opens up the opportunity for further exploration into different modes of binding of the compound onto surfaces of medical importance. Future studies are planned to include *in vitro* release kinetics of the peptidomimetics from HA as well as challenge models in mice and a rabbit distal femoral defect model. The results from this study paves the way for further exploration of different antibacterial peptidomimetics on HA surfaces.

Author contributions

N. K., M. W., I. R., R. C., B. W., R. K., and S. C. conceptualized the study, S. C. and R. K. conducted *in vitro* experiments and analyzed the data, N. K., M. W., I. R., and R. C. analyzed the data, S. C. and R. K. drafted the manuscript.

Conflicts of interest

There are no conflicts to declare.

Acknowledgements

The authors would like to acknowledge the electron microscopy unit and the spectroscopy unit at Mark Wainwright Analytical Centre, UNSW Sydney for providing the SEM imaging, and FT-IR, RAMAN spectroscopy facilities, respectively. Sudip Chakraborty would like to acknowledge the Graduate Research School, UNSW Sydney, for providing him with the Tuition Fee Scholarship for pursuing his research degree. This work was supported by the NHMRC [APP1183597].

References

- 1 T. F. Moriarty, R. Kuehl, T. Coenye, W. J. Metsemakers, M. Morgenstern, E. M. Schwarz, M. Riool, S. A. J. Zaai, N. Khana, S. L. Kates and R. G. Richards, *EFORT Open Rev.*, 2016, **1**, 89–99.
- 2 R. Spitzmüller, D. Gumbel, C. Güthoff, S. Zaatreh, A. Klinder, M. Napp, R. Bader, W. Mittelmeier, A. Ekkernkamp, A. Kramer and D. Stengel, *BMC Musculoskeletal Disord.*, 2019, **20**, 184.
- 3 G. Tsaras, D. R. Osmon, T. Mabry, B. Lahr, J. St Sauveur, B. Yawn, R. Kurland and E. F. Berbari, *Infect. Control Hosp. Epidemiol.*, 2012, **33**, 1207–1212.
- 4 A. Patel, G. Pavlou, R. E. Mújica-Mota and A. D. Toms, *Bone Joint J.*, 2015, **97-b**, 1076–1081.
- 5 R. E. Delanois, J. B. Mistry, C. U. Gwam, N. S. Mohamed, U. S. Choksi and M. A. Mont, *J. Arthroplasty*, 2017, **32**, 2663–2668.
- 6 K. J. Bozic, E. Lau, S. Kurtz, K. Ong, H. Rubash, T. P. Vail and D. J. Berry, *J. Bone Jt. Surg., Am. Vol.*, 2012, **94**, 794–800.
- 7 E. Sullivan, A. Gupta and C. H. Cook, *Surg. Infect.*, 2017, **18**, 451–454.
- 8 M. J. Patzakis and J. Wilkins, *Clin. Orthop. Relat. Res.*, 1989, 36–40.
- 9 B. Sugarman and E. J. Young, *Infect. Dis. Clin. North Am.*, 1989, **3**, 187–198.
- 10 W. Zimmerli, A. Trampuz and P. E. Ochsner, *N. Engl. J. Med.*, 2004, **351**, 1645–1654.
- 11 M. Saadatian-Elahi, R. Teyssou and P. Vanhems, *Int. J. Surg.*, 2008, **6**, 238–245.
- 12 S. M. Kurtz, E. Lau, J. Schmier, K. L. Ong, K. Zhao and J. Parvizi, *J. Arthroplasty*, 2008, **23**, 984–991.
- 13 S. Corvec, M. E. Portillo, B. M. Pasticci, O. Borens and A. Trampuz, *Int. J. Artif. Organs*, 2012, **35**, 923–934.
- 14 J. L. Del Pozo and R. Patel, *N. Engl. J. Med.*, 2009, **361**, 787–794.
- 15 L. Montanaro, P. Speziale, D. Campoccia, S. Ravaioli, I. Cangini, G. Pietrocola, S. Giannini and C. R. Arciola, *Future Microbiol.*, 2011, **6**, 1329–1349.
- 16 A. Trampuz and W. Zimmerli, *Injury*, 2006, **37**(Suppl 2), S59–S66.
- 17 A. J. Tande and R. Patel, *Clin. Microbiol. Rev.*, 2014, **27**, 302–345.
- 18 E. Klein, D. L. Smith and R. Laxminarayan, *Emerg. Infect. Dis. J.*, 2007, **13**, 1840.
- 19 A. G. Jensen, C. H. Wachmann, K. B. Poulsen, F. Espersen, J. Scheibel, P. Skinhøj and N. Frimodt-Møller, *Arch. Intern. Med.*, 1999, **159**, 1437–1444.
- 20 C.-J. Kim, H.-B. Kim, M.-D. Oh, Y. Kim, A. Kim, S.-H. Oh, K.-H. Song, E. S. Kim, Y. K. Cho, Y. H. Choi, J. Park, B.-N. Kim, N.-J. Kim, K.-H. Kim, E. J. Lee, J.-B. Jun, Y. K. Kim, S. M. Kiem, H. J. Choi, E. J. Choo, K.-M. Sohn, S. Lee, H. H. Chang, J. H. Bang, S. J. Lee, J. H. Lee, S. Y. Park, M. H. Jeon, N. R. Yun and K. S. G. The, *BMC Infect. Dis.*, 2014, **14**, 590.
- 21 C. L. Ventola, *P T*, 2015, **40**, 277–283.
- 22 D. Teterycz, T. Ferry, D. Lew, R. Stern, M. Assal, P. Hoffmeyer, L. Bernard and I. Uçkay, *Int. J. Infect. Dis.*, 2010, **14**, e913–e918.
- 23 J. Conly and B. Johnston, *Can. J. Infect. Dis. Med. Microbiol.*, 2005, **16**, 159–160.
- 24 M. I. Hutchings, A. W. Truman and B. Wilkinson, *Curr. Opin. Microbiol.*, 2019, **51**, 72–80.



- 25 B. Li and T. J. Webster, *J. Orthop. Res.*, 2018, **36**, 22–32.
- 26 H. W. Boucher, G. H. Talbot, D. K. Benjamin, Jr., J. Bradley, R. J. Guidos, R. N. Jones, B. E. Murray, R. A. Bonomo, D. Gilbert and A. Infectious Diseases Society of, *Clin. Infect. Dis.*, 2013, **56**, 1685–1694.
- 27 J. A. DiMasi, H. G. Grabowski and R. W. Hansen, *J. Health Econ.*, 2016, **47**, 20–33.
- 28 L. J. Piddock, *Lancet Infect. Dis.*, 2012, **12**, 249–253.
- 29 J. G. Bartlett, D. N. Gilbert and B. Spellberg, *Clin. Infect. Dis.*, 2013, **56**, 1445–1450.
- 30 M. Magana, M. Pushpanathan, A. L. Santos, L. Leanse, M. Fernandez, A. Ioannidis, M. A. Giulianotti, Y. Apidianakis, S. Bradfute, A. L. Ferguson, A. Cherkasov, M. N. Seleem, C. Pinilla, C. de la Fuente-Nunez, T. Lazaridis, T. Dai, R. A. Houghten, R. E. W. Hancock and G. P. Tegos, *Lancet Infect. Dis.*, 2020, **20**, e216–e230.
- 31 N. Mookherjee and R. E. Hancock, *Cell. Mol. Life Sci.*, 2007, **64**, 922–933.
- 32 R. E. Hancock and D. S. Chapple, *Antimicrob. Agents Chemother.*, 1999, **43**, 1317–1323.
- 33 M. Kazemzadeh-Narbat, J. Kindrachuk, K. Duan, H. Jenssen, R. E. W. Hancock and R. Wang, *Biomaterials*, 2010, **31**, 9519–9526.
- 34 M. Kazemzadeh-Narbat, S. Noordin, B. A. Masri, D. S. Garbuz, C. P. Duncan, R. E. W. Hancock and R. Wang, *J. Biomed. Mater. Res., Part B*, 2012, **100B**, 1344–1352.
- 35 M. Kazemzadeh-Narbat, B. F. L. Lai, C. Ding, J. N. Kizhakkedathu, R. E. W. Hancock and R. Wang, *Biomaterials*, 2013, **34**, 5969–5977.
- 36 L. Townsend, R. L. Williams, O. Anuforum, M. R. Berwick, F. Halstead, E. Hughes, A. Stamboulis, B. Oppenheim, J. Gough, L. Grover, R. A. H. Scott, M. Webber, A. F. A. Peacock, A. Belli, A. Logan and F. de Cogan, *J. R. Soc., Interface*, 2017, **14**, 20160657.
- 37 A. Rozek, J.-P. S. Powers, C. L. Friedrich and R. E. W. Hancock, *Biochemistry*, 2003, **42**, 14130–14138.
- 38 I. H. Lee, Y. Cho and R. I. Lehrer, *Infect. Immun.*, 1997, **65**, 2898–2903.
- 39 T. Rydlo, S. Rotem and A. Mor, *Antimicrob. Agents Chemother.*, 2006, **50**, 490.
- 40 A. K. Marr, W. J. Gooderham and R. E. Hancock, *Curr. Opin. Pharmacol.*, 2006, **6**, 468–472.
- 41 R. Kuppusamy, M. Yasir, E. Yee, M. Willcox, D. S. Black and N. Kumar, *Org. Biomol. Chem.*, 2018, **16**, 5871–5888.
- 42 R. Kuppusamy, M. Yasir, T. Berry, C. G. Cranfield, S. Nizalapur, E. Yee, O. Kimyon, A. Taunk, K. K. K. Ho, B. Cornell, M. Manefield, M. Willcox, D. S. Black and N. Kumar, *Eur. J. Med. Chem.*, 2018, **143**, 1702–1722.
- 43 Z. Bal, T. Kaito, F. Korkusuz and H. Yoshikawa, *Emergent Mater.*, 2019, **3**, 521–544.
- 44 S. D. Cook, J. E. Dalton, E. H. Tan, W. V. Tejeiro, M. J. Young and T. S. Whitecloud, 3rd, *Spine*, 1994, **19**, 1856–1866.
- 45 H. J. Senter, R. Kortyna and W. R. Kemp, *Neurosurgery*, 1989, **25**, 39–43.
- 46 S. Allegrini, Jr., E. Rumpel, E. Kauschke, J. Fanghanel and B. Konig, Jr., *Ann. Anat.*, 2006, **188**, 143–151.
- 47 W. S. W. Harun, R. I. M. Asri, A. B. Sulong, S. A. C. Ghani and Z. Ghazalli, *Hydroxyapatite – Advances in Composite Nanomaterials, Biomedical Applications and Its Technological Facets*, 2018, DOI: 10.5772/intechopen.71063ch. 5.
- 48 C. J. Oosterbos, H. Vogely, M. W. Nijhof, A. Fleer, A. J. Verbout, A. J. Tonino and W. J. Dhert, *J. Biomed. Mater. Res.*, 2002, **60**, 339–347.
- 49 M. Wu, E. Maier, R. Benz and R. E. W. Hancock, *Biochemistry*, 1999, **38**, 7235–7242.
- 50 G. A. O'Toole, *J. Vis. Exp.*, 2011, 2437, DOI: 10.3791/2437.
- 51 M. Balouiri, M. Sadiki and S. K. Ibnsouda, *J. Pharm. Anal.*, 2016, **6**, 71–79.
- 52 L. Deng, Y. Deng and K. Xie, *Colloids Surf., B*, 2017, **160**, 483–492.
- 53 B. Mojsoska and H. Jenssen, *Pharmaceuticals*, 2015, **8**, 366–415.
- 54 N. Høiby, T. Bjarnsholt, M. Givskov, S. Molin and O. Ciofu, *Int. J. Antimicrob. Agents*, 2010, **35**, 322–332.
- 55 Y. He, Y. Jin, X. Ying, Q. Wu, S. Yao, Y. Li, H. Liu, G. Ma and X. Wang, *Regener. Biomater.*, 2020, **7**, 515–525.
- 56 L. Chen, L. Shao, F. Wang, Y. Huang and F. Gao, *RSC Adv.*, 2019, **9**, 10494–10507.
- 57 Z. Ye, X. Zhu, I. Mutreja, S. K. Boda, N. G. Fischer, A. Zhang, C. Lui, Y. Qi and C. Aparicio, *Bioact. Mater.*, 2021, **6**, 2250–2260.
- 58 C. T. Johnson and A. J. García, *Ann. Biomed. Eng.*, 2015, **43**, 515–528.
- 59 J. R. Sharpe, R. L. Sammons and P. M. Marquis, *Biomaterials*, 1997, **18**, 471–476.
- 60 D. M. Ibrahim, E. S. Sani, A. M. Soliman, N. Zandi, E. Mostafavi, A. M. Youssef, N. K. Allam and N. Annabi, *ACS Appl. Bio Mater.*, 2020, **3**, 3313–3325.

